DOI: 10.1002/ejic.201001264

$\{Rh(PiBu_3)_2\}^+$ Fragments Ligated to Arenes: From Benzene to Polyaromatic Hydrocarbons, Part II[‡] – Computational Analysis of Pathways for Haptotropic Migration

Anthony Woolf,[a] Muhsen A. M. Alibadi,[a] Adrian B. Chaplin,[a] John E. McGrady,*[a] and Andrew S. Weller[a]

Keywords: Density functional calculations / Rhodium / Arene ligands / Arenes / Pi interactions / Hydrocarbons / Polyaromatic hydrocarbons

Density functional theory has been used to probe the structures and solution dynamics of a series of polyaromatic hydrocarbon complexes of the 12-electron fragment $\{Rh(PiBu_3)_2\}^+$. These studies suggest that the strength of the binding of the metal to the hydrocarbon surface is controlled by the electronic demands of both the metal (16-electron configuration) and ligand (maximum retention of aromaticity). In cases where these two factors can be satisfied simultaneously an energetically isolated equilibrium structure emerges and haptotropic shifts are blocked. In cases where a compromise between the requirements of the metal and ligand is unavoidable the potential energy surface is rather flatter, leading to rapid haptotropic shifts between near iso-energetic isomers.

Introduction

In Part I[1] of this series we have highlighted the subtle variations in structure and dynamics across a series of closely related complexes of the $\{Rh(PiBu_3)_2\}^+$ fragment with polyaromatic hydrocarbons (PAH) (Figure 1). We now present an analysis of the electronic structure of these complexes using density functional theory, and in so doing provide a framework for understanding both the equilibrium structures and fluxional processes. The factors that determine barriers to migratory processes in complexes of the $Cr(CO)_3$ fragment were first set out by Albright and coworkers using extended Hückel theory.[2] Since that initial work numerous studies have used density functional theory to compute minimum energy pathways for haptotropic shifts for PAHs[3–6] and also carbon nanotubes.[7] Analogous processed in isolobal $M(PR_3)_3$[8] and M(Cp)[9] (M = Cr, Mo, W) have also been discussed. Albright has also identified the key differences between ML_3 fragments and their ML_2 analogues (such as the $\{Rh(PR_3)_2\}^+$ of direct interest here).[10] Most pertinently, the d^6 ML_3 fragment has a degenerate pair of vacant M–L antibonding orbitals that interact strongly with the π system of the PAH while the d^8 ML_2 fragment has only one, and this proves to have a significant impact on both structure and dynamics.

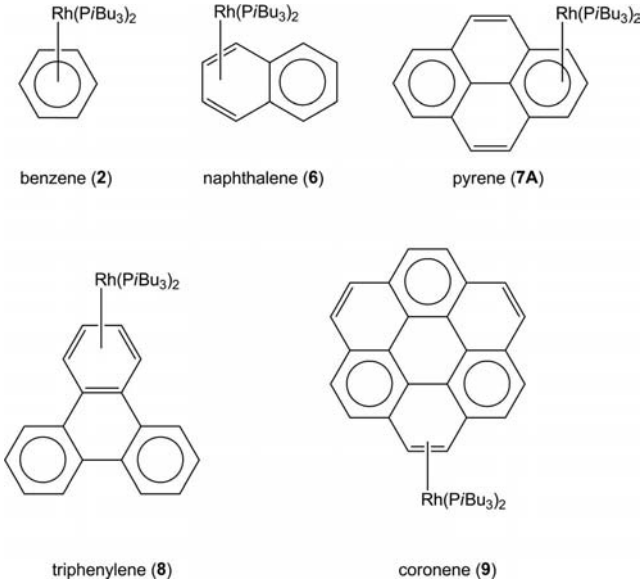

Figure 1. PAH complexes of $\{Rh(PiBu_3)_2\}^+$ characterised in ref.[1]

Electronic Structure: General Considerations

The crystallographic data summarized in ref.[1] reveals a rich coordination chemistry, with η^2 (coronene **10**), η^3 (pyrene **7A**), η^4 (naphthalene **4**, anthracene **5**, triphenylene **8**) and η^6 (benzene, **2**, **3**) coordination modes. In general, the equilibrium geometry of any complex will reflect a compromise between the electronic demands of the metal (the balance between 16- or 18-electron configurations), those of the ligand (retention of maximum resonance delocalization

[‡] Part I: Ref.[1]

[a] Department of Chemistry, Inorganic Chemistry Laboratories, Oxford, OX1 3QR, UK
E-mail: andrew.weller@chem.ox.ac.uk
john.mcgrady@chem.ox.ac.uk

Supporting information for this article is available on the WWW under http://dx.doi.org/10.1002/ejic.201001264.

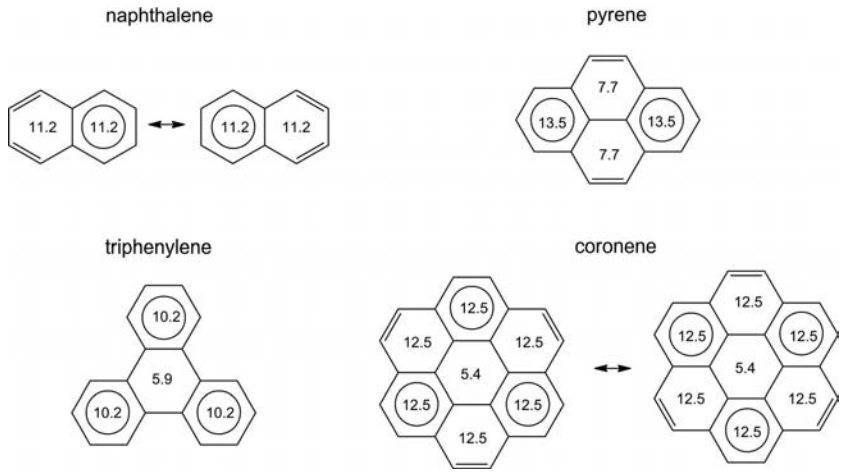

Scheme 1. Clar structures for naphthalene, pyrene, triphenylene and coronene. NICS(1) values are inscribed.

in the π system) and the minimization of steric repulsions between the metal fragment and the planar aromatic ring. Clar's protocol for defining the dominant resonance form in such structures provides useful guidelines regarding the availability of π electron density. Clar proposed that the dominant resonance form in any PAH structure corresponds to that with the greatest number of disjoint benzenoid sextets (Scheme 1)[11] Computed Nucleus Independent Chemical Shift [NICS(1)] values, which have been used extensively to interpret changes in aromaticity, are inscribed inside each of the six-membered rings – higher values indicate greater aromatic delocalization of the π system.[12,13] In each case, coordination of one or more double bonds to a metal centre necessarily implies some degree of disruption of the resonance-delocalized π system of the PAH. A general tendency to coordinate a metal fragment at the least substituted ring, which tends to be the most aromatic, has been noted by other authors.[14] Donation of four electrons from either naphthalene or triphenylene in a butadiene-like motif will disrupt the aromaticity of only one isolated ring. For coronene, in contrast, the dominant Clar structures indicate that it will be impossible to donate four electrons in a butadiene motif to the metal without disrupting the π delocalization in two adjacent rings. This emphasizes the point that the electronic demands of metal and ligand are often in conflict, and the equilibrium structure must inevitably represent some form of compromise. The NMR spectroscopic data are similarly rich, revealing processes that allow the $\{Rh(P\textit{i}Bu_3)_2\}^+$ fragment to (i) rotate about the axis connecting the metal to the aromatic ring, equalizing the methyl groups of the diastereotopic *i*Bu groups and (ii) migrate between rings in a series of haptotropic shifts.

As a prelude to our survey of the complexes of PAHs, we first establish the structural preferences of the $\{Rh(PMe_3)_2\}^+$ fragment when bonded to model hydrocarbon fragments, C_2H_4 (η^2-ethene), $C_3H_5^-$ (η^3-allyl), C_4H_6 (η^4-butadiene) and C_6H_6 (η^6-benzene). These structural archetypes provide convenient benchmarks, deviations from which must reflect the influence of the delocalized π framework of the extended PAH ligand. In all cases the *i*Bu substituents on the phosphane ligands have been replaced with more computationally tractable methyl groups.

Model Complexes of Ethene, Allyl Anion, Butadiene and Benzene

The optimised structures of the ethene (**Eth1**), allyl (**Allyl1**), butadiene (**But1**) and benzene (**Benz1**) complexes of $\{Rh(PMe_3)_2\}^+$ are summarized in Figure 2. The metal centre in **Eth1** adopts a T-shaped geometry, typical of 14-electron fragments of this type.[7] One of the phosphane ligands lies *trans* to the vacant site leading to distinctly different Rh–P bond lengths, the one *trans* to ethene being longer by 0.14 Å (2.35 vs. 2.21 Å). The ethene ligand lies perpendicular to the RhP_2 plane, with two equivalent Rh–C bond lengths of 2.17 Å. In the neutral allyl complex, **Allyl1**, the rhodium adopts an approximately square-planar coordination geometry typical of a 16-electron configuration. The allyl unit sits perpendicular to the P–Rh–P plane and occupies two mutually *cis* sites with $Rh–C_{terminal}$ and $Rh–C_{central}$ bond lengths of 2.19 and 2.14 Å, respectively. The Rh–P bond lengths are also identical at 2.29 Å. Approximately square-planar coordination is also apparent in the 16-electron butadiene complex, **But1**. The Rh–C distances to the inner two carbon atoms are somewhat shorter than those to the terminal atoms (2.17 vs. 2.26 Å), and there is a distinct hinging (defined as the C–C–C–H torsion angle) of 31.8° at the terminal CH_2 groups associated with the rehybridisation at the carbons (H atoms are not shown in the figure). The Rh–P bonds are equivalent at 2.35 Å, some 0.06 Å longer than those in the allyl analogue. The basic features of **Benz1** are very similar to those obtained from the diffraction experiment (**2**). The optimized Rh–C bond lengths span a narrow range from 2.33–2.39 Å, consistent with an η^6 coordination mode and an 18-electron configuration at the metal. However, whilst the deviations from the mean are small, they do reveal a distinct tendency towards

square-planar coordination: one pair of mutually *trans* carbon atoms is displaced away from the metal (Rh–C 2.39 Å), leaving two pairs of bonded carbons (Rh–C 2.33 Å) to complete the coordination sphere. The discussion of the benzene complex neatly highlights the fact that an unambiguous assignment of hapticity, and therefore electron count at the metal, is not always straightforward – we return to this point in the discussion of the naphthalene complexes.

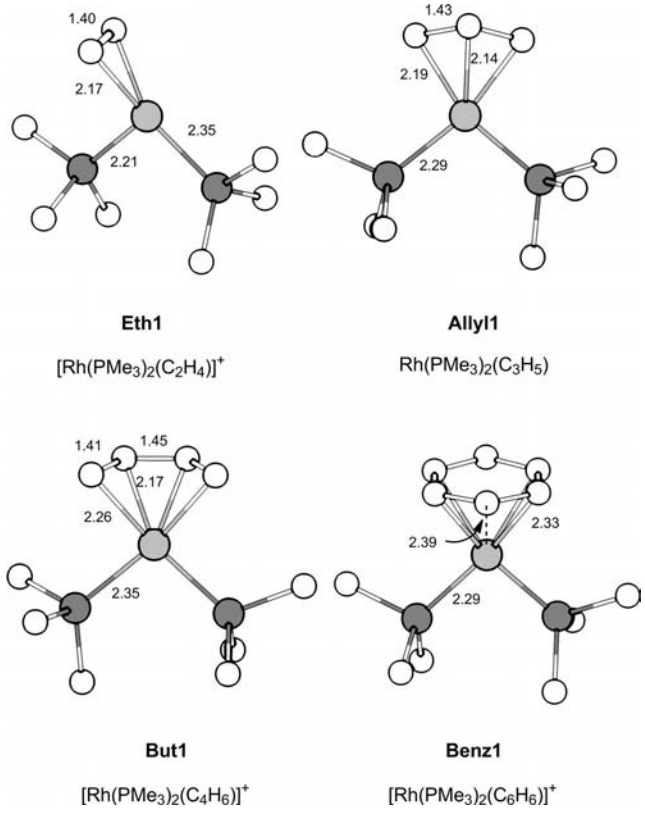

Figure 2. Optimised structures of the ethene, allyl, butadiene and benzene complexes of $\{Rh(PMe_3)_2\}^+$.

Complexes of Naphthalene, Pyrene, Triphenylene and Coronene

Naphthalene: $[Rh(PMe_3)_2(C_{10}H_8)]^+$

The global minimum for the naphthalene complex, **Nap1** (Figure 3) has four short Rh–C bonds in the range 2.23–2.31 Å, suggesting an η^4-coordination mode, although the hinge angle (13.9°) is rather small and the non-bonded Rh–C distances of 2.71 Å are only ca. 0.4 Å longer. The qualitative nature of this "ring slippage" is identical to that noted in early work on the $Cr(CO)_3$ complex of naphthalene,[2,4,8] although the hinging is less pronounced in that case (5.5°) as is the distinction between bonded- and nonbonded M–C distances (ΔCr–C 0.12 Å). The hapticity in the chromium case has been assigned as "slipped η^6" rather than η^4.[2] The origin of this slip can be traced to the nodal characteristics of the HOMO and HOMO-1 of the naphthalene ligand (Scheme 2) which interact with the two vacant Cr–CO antibonding orbitals. The presence of a node at the central C–C unit in the HOMO reduces the overlap with the *xz* component, resulting in a slip towards the outer C=C bond. In d^8 ML_2 fragment such as $\{Rh(PR_3)_2\}^+$ there is only a single vacant Rh–P antibonding orbital (d_{yz}) and so interactions with the HOMO-1 are repulsive ("filled-filled"). The result is more pronounced slippage, the limit of which is the square-planar η^4-coordination mode and 16-electron configuration apparent in **Nap1**. Structural comparisons with naphthalene complexes of 14-electron fragments such as $Rh(\eta^5\text{-}C_5Me_5)$ and $Ru(PEt_3)(\eta^4\text{-COD})$ are also revealing. In these examples of unambiguous η^4-coordination the hinge angle is substantially larger (35[15] and 41.5°,[16] respectively), as is the difference between bonded and non-bonded M–C distances (ca. 0.7 Å). The structural parameters for **Nap1** (13.9°) therefore suggest that it lies somewhere between the limits of η^6 and η^4 coordination defined by $Cr(CO)_3(\eta^6\text{-naphthalene})$ (5.5°) and $Rh(\eta^5\text{-}C_5Me_5)(\eta^4\text{-naphthalene})$ (35°), respectively. On this basis we view the hapticity in **Nap1** as η^4 but acknowledge that there is clearly some interaction of the π electron density on the central C–C unit with the vacant p orbital on the Rh centre (the orbital that is strictly non-bonding in an ideal square-planar environment) which reduces the hinge angle compared to 18-electron η^4 complexes.

The NMR spectroscopic data reported for **4** demonstrate that (i) a low-energy dynamic process that interconverts the diastereotopic Me groups of the *i*Bu ligands is operative and (ii) haptotropic shifts that would allow the Rh fragment to migrate from one ring to another are *not* accessible at room temperature. For the first of these processes we have located a transition state for rotation about the pseudo-C_6 axis of the coordinated ring, **NapTS1**, only 8.3 kcal/mol above the equilibrium structure and consistent with the room temperature fluxionality of **4**. In **NapTS1** the RhP_2 plane is aligned parallel to the long axis of the naphthalene unit with one Rh–P bond directly below the aromatic ring and the other directed outwards. Consistent with this, the metal fragment adopts a distinctly T-shaped geometry (Rh–P 2.26 and 2.30 Å), suggesting a slip towards η^2 coordination as in **Eth1**. Thus the rotation of the RhP_2 fragment appears to involve an η^4-η^2-η^4 pathway. Albright et al. have highlighted a similar pathway for the $Cr(CO)_3$ complex, and noted that trapping of the coordinatively unsaturated metal center in the intermediate may lead to dissociation.[2]

A number of authors have considered pathways for haptotropic shifts in naphthalene using Extended Hückel and density functional methods,[2–7,10] and all agree that a direct migration across the centre of the C–C bond linking the two rings is not viable. The origins of the high barrier have been traced to destabilizing interactions between the HOMO and a filled metal orbital. Consistent with this, a structure where the $\{Rh(PMe_3)_2\}^+$ fragment sits in this position corresponds to a second-order saddle point, 22.7 kcal/mol above the equilibrium structure. Instead, we find that the lowest energy pathway involves an intermediate structure, **Nap2**, where the RhP_2 fragment coordinates in an η^3-mode to three carbons, the central one lying at the

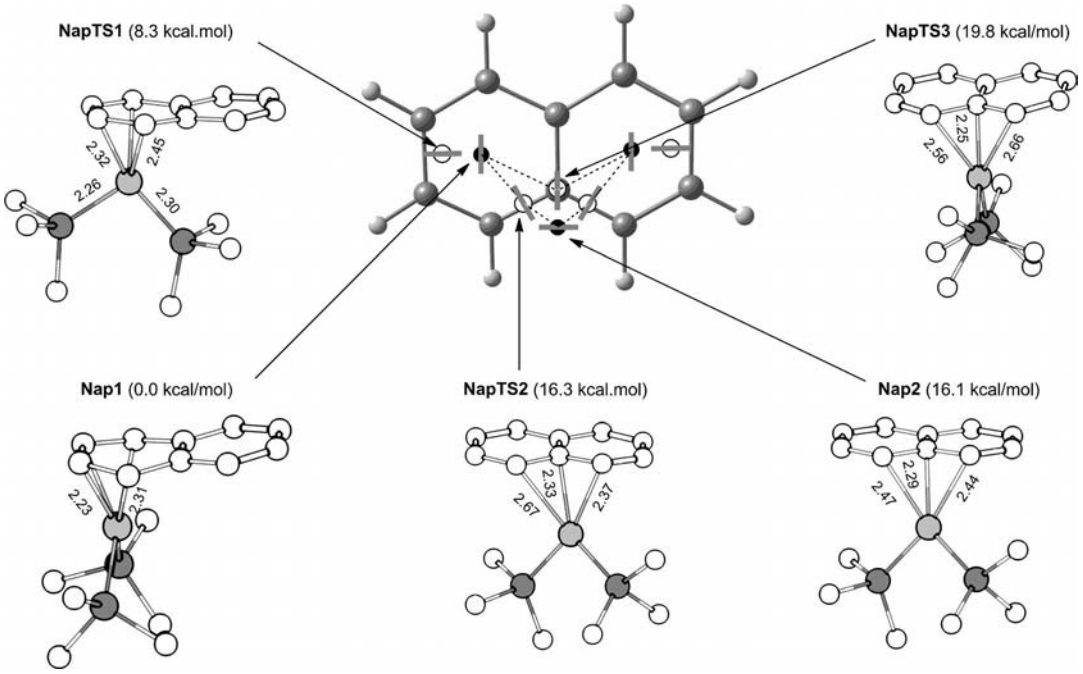

Figure 3. Schematic potential energy surface and structures of stationary points for the naphthalene complex. Minima and transition states are shown as filled and empty circles, respectively. Red lines indicate the alignment of the Rh–P bonds.

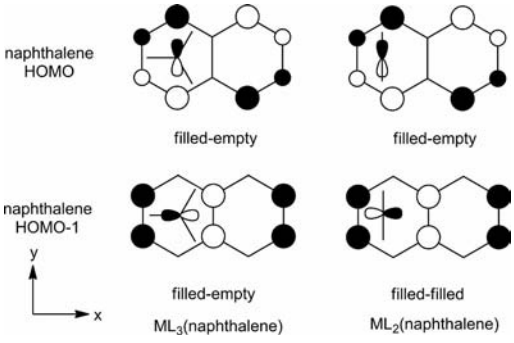

Scheme 2. Frontier molecular orbital overlaps for ML_3 (d^6) and ML_2 (d^8) complexes of naphthalene.[2]

junction of the two six-membered rings. The equivalent Rh–P bond lengths are typical of an η^3 structure while the Rh–C bond lengths (2.29 and 2.45 Å) are somewhat longer than those in **Allyl1**, the complex of $C_3H_5^-$. **Nap2** lies 16.1 kcal/mol above the two equivalent η^4-coordinated equilibrium structures, and is connected to them by two equivalent transition states, **NapTS2**, that lie only 0.2 kcal/mol above **Nap2**. The very late transition state can also be considered as η^3-coordinated, albeit with a distinct asymmetry in the terminal Rh–C distances. The pathway connecting the two degenerate equilibrium η^4 structures via **Nap2** therefore involves a glide across the surface with a concomitant rotation of the RhP_2 fragment. We have also located a third transition state, **NapTS3** (located by following the lower of the imaginary frequencies in the second order saddle point identified above), that links the two equivalent equilibrium structures directly. Based on the large difference between Rh–C distances (2.25 and about 2.60 Å) in **NapTS3** we assign the coordination mode as η^1, although Dolg and coworkers have described similar structures as η^4-(trimethylenemethane).[5] The P–Rh–P plane in **NapTS3** is rotated by 90° relative to **Nap2**, and contains the central C–C bond. The migration of the metal centre across the naphthalene surface via **NapTS3** therefore involves a simple glide, with no concomitant rotation of the RhP_2 unit. **NapTS3** lies a further 3.5 kcal/mol above **NapTS2**, suggesting that migration and rotation are coupled in the least energy pathway. The rate-determining barrier to the migratory process is therefore 16.3 kcal/mol – we defer a comparison between experiment and theory until we have described the analogous pathways for the larger PAH ligands.

Before moving on to more complex PAHs, it is useful to compare our computed pathway with previous work on the $Cr(CO)_3$ system. Based on extended Hückel theory, Albright et al. anticipated the presence of η^3-intermediate analogous to **Nap2**[2] but subsequent work using DFT failed to locate this as a local minimum.[3–5] The lowest energy pathway instead passes through an η^1-transition state, analogous to **NapTS3**. The presence of the η^3-intermediate in the case of $\{(RhPMe_3)_2\}^+$ but not $Cr(CO)_3$ can again be explained by the presence of two vacant M–L antibonding orbitals in the latter but only one in the former. Thus in a putative η^3-intermediate of $Cr(CO)_3$, overlap between the empty d_{yz} orbital and the HOMO-1 will pull the metal fragment back towards the centre of the aromatic system (Scheme 3). In the $\{(RhPMe_3)_2\}^+$ case the corresponding interaction is repulsive (filled-filled), pushing the metal fragment towards the outside of the ring. Only in larger PAHs, where donation from an additional carbon-centre p

orbital on the opposite side of the metal fragment is possible, are η^3-intermediates located for $Cr(CO)_3$.[3,4] Our computed barrier of 16.3 kcal/mol is significantly lower than the value of 25.7 kcal/mol reported by Sola and coworkers,[3,4] reflecting the fact that a 16-electron count at Rh is effectively maintained throughout the process, whereas the electron count at Cr must inevitably change during the migration.

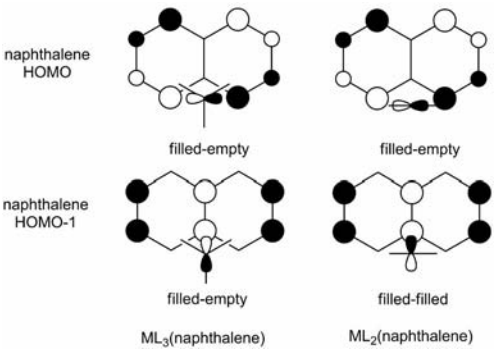

Scheme 3. Orbital interactions in η^3 allyl intermediates.

Pyrene: $[Rh(PMe_3)_2(C_{16}H_{10})]^+$

The potential energy landscape for the pyrene system is a complex one, with three structurally distinct minima (**Pyr1**, **Pyr2** and **Pyr3**) lying within 1 kcal/mol of each other. The presence of a single resonance in the ^{31}P NMR spectrum of the dominant isomer, **7A**, suggests either that the metal fragment coordinates in a η^3-fashion or that equivalent η^2 structures (as found in the solid state) interconvert rapidly on the NMR timescale. The global minimum, **Pyr1**, corresponds to an η^3-structure with the metal binding to the three non-fused carbon atoms of one of the outer rings. The presence of two identical $Rh–C_{terminal}$ bond lengths that are marginally longer than $Rh–C_{central}$ is characteristic of allyl-like coordination, as are the identical Rh–P bond lengths and the orientation of the ligand relative to the P–Rh–P plane. The structural features are very similar to those of the complex of the isolated $C_3H_5^-$ fragment, **Allyl1**, although the Rh–C distances are ca. 0.1 Å longer indicating that the pyrene unit is somewhat more weakly bound. We have also located a second closely related structure, **Pyr2**, where the metal adopts an η^2-coordinated geometry similar to that in the crystal structure. The inequivalent Rh–P bond lengths and T-shaped geometry are reminiscent of the ethene complex, **Eth1**. **Pyr2** lies only 1.2 kcal/mol above **Pyr1**, and the two are connected by a very minor slip of the allyl unit. We have been unable to locate a transition state connecting **Pyr1** and **Pyr2**, suggesting that they may simply correspond to different regions of a rather flat potential energy well rather than distinct minima. In any case, the metal centre will be free to move along the C_3 unit with little energetic cost, and subtle intermolecular effects in the extended crystal lattice may impose the observed geometry. We note in this context that Stanger has identified two independent units in the crystal structure the Ni(depe)(anthracene) [depe = 1,2-bis(diethylphosphanyl)ethane], one with a η^3 coordination mode and the other η^4.[17]

The solution NMR spectroscopic data discussed in Part I indicate the presence of a second quite distinct pyrene isomer, **7B**, lying only 0.5 kcal/mol above **7A**. Based on the observed ^{31}P chemical shifts we proposed a structure where the metal was coordinated to one of the inner rings of the pyrene unit. Consistent with this proposal, we have located a third minimum, **Pyr3**, 1.1 kcal/mol above **Pyr1** (and therefore almost isoenergetic with **Pyr2**) where the metal is coordinated in an η^2-mode to a double bond of one of the central rings. The metal in **Pyr3** adopts a T-shaped geometry characteristic of η^2-coordination, with two quite distinct Rh–P bond lengths (2.23 and 2.33 Å vs. 2.21 and 2.35 Å in **Eth1**) and a coordinated C=C unit perpendicular to the P–Rh–P plane.

The computed potential energy surface in the region linking **Pyr1** and **Pyr3** is qualitatively similar to that found for naphthalene, except that the two end points are no longer degenerate. We again find two distinct pathways linking the minima, one corresponding to a simple glide, the other to a glide combined with a rotation of the RhP_2 unit. The lower energy of the two (glide + rotation) passes through an η^3-coordinated intermediate, **Pyr4** lying 9.6 kcal/mol above **Pyr1** (cf. 16.1 kcal/mol for **Nap2**). The local structures about the metal in **Nap2** and **Pyr4** are strikingly similar, with a short Rh–C bond to the central carbon of the allyl unit (2.25 Å in **Pyr4** vs. 2.29 Å in **Nap2**) and two rather longer bonds to the outer carbons (2.38 and 2.50 Å in **Pyr4**, 2.44 and 2.47 Å in **Nap2**). The coordination about the metal is approximately square planar in both cases. The intervening transition states, **PyrTS1** and **PyrTS2** lie 11.7 kcal/mol and 10.2 kcal/mol above **Pyr1**, respectively, and are structurally very similar to the intermediate, **Pyr4**. They also resemble closely the naphthalene analogue, **NapTS2**. The computed barrier of 11.7 kcal/mol for the haptotropic shift in pyrene (**PyrTS1**) is in excellent agreement with the experimentally determined value of $\Delta H^{\ddagger} = 11.1 \pm 0.8$ kcal/mol and is substantially lower than the corresponding process in the naphthalene analogue (**NapTS2**, 16.3 kcal/mol) where no evidence for fluxionality has been detected.

The presence of multiple minima of similar energy on the pyrene potential energy surface stands in stark contrast to the energetically isolated equilibrium structure of the naphthalene analogue, and reflects the inevitable compromises involved in the coordination of pyrene to a 12-electron $[Rh(PMe_3)_2]^+$. The Clar structure in Scheme 1 shows that only isolated C=C bonds are present outside resonant sextets in the dominant structure, and so adoption of an η^4 geometry, with its desirable 16-electron count at the metal, must necessarily disrupt the aromaticity to a significant extent. The influence of coordination of a transition metal on the aromaticity of a ring has been debated,[18] with some authors arguing for an increase, others for a decrease. Our focus here is, however, on the aromaticity of the remainder of the conjugated π system that is *not* directly bound to the metal. The NICS values shown inset in Figure 4 indicate that for **Pyr3**, the aromaticity of the two outer rings is al-

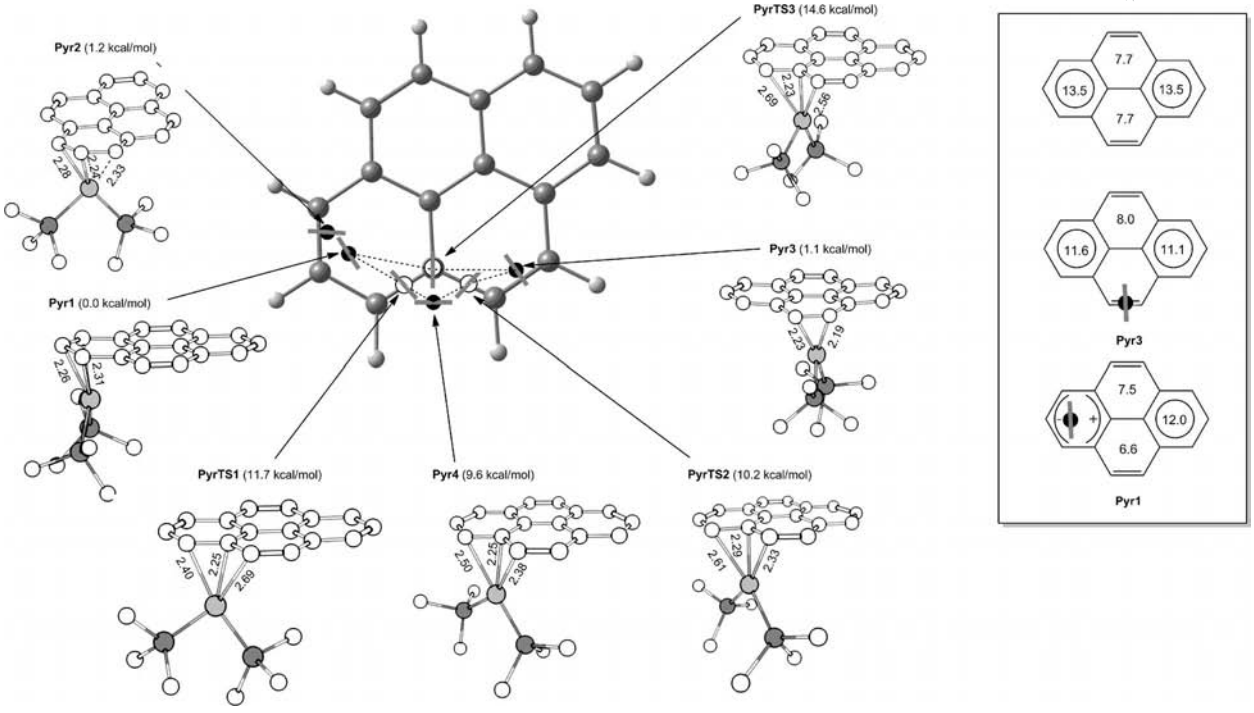

Figure 4. Schematic potential energy surface and structures of stationary points for the pyrene complex. NICS(1) values for the uncoordinated rings in key minima are shown in the inset.

most undiminished relative to the free ligand, but the trade off is a highly unsaturated 14-electron rhodium centre. In **Pyr1**, in contrast, the metal does achieve the more stable 16-electron count, but only at the expense of accessing a less stable zwitterionic resonance form of the ligand with substantial loss of aromaticity.

Triphenylene: $[Rh(PMe_3)_2(C_{18}H_{12})]^+$

The potential energy surface for the triphenylene complex (Figure 5) resembles the naphthalene case in so much as the global minimum, **Trip1**, is energetically isolated, lying more than 10 kcal/mol below any other stationary point. The optimized structure of **Trip1** shows a typical η^4-coordination geometry, very similar to the X-ray counterpart, with four short (2.27–2.30 Å) Rh–C bonds. The degree of hinging (10.5°) is much smaller than the 43.1° observed in Ru(η^4-triphenylene)($PMe_2Ph)_3$,[19] consistent with 16 electron/18 electron arguments described previously. More subtley, it is even smaller than that observed for naphthalene (13.9°), leaving the non-bonding carbons even closer to the metal (2.57 vs. 2.71 Å). This difference reflects the resonance delocalization in the important Clar structures. In the naphthalene case the non-bonded C=C π bond (that links the two rings) is involved in a resonant sextet, and therefore is less accessible than the corresponding C=C π bond in triphenylene, which is *not*. Thus the resonance delocalization of the additional C=C bond appears to have a significant impact on the balance between 16-electron and 18-electron configurations at the metal.

In contrast to Sola's work on $Cr(CO)_3$, we have been unable to locate any minimum where the metal fragment is coordinated in an η^6 fashion to the central ring. All attempts instead resulted in a slip of the metal centre towards one of the "bays" in the triphenylene structure, resulting in an η^4-coordinated structure, **Trip2**. The difference between the two systems again has its origins in the presence of two vacant, mutually orthogonal M–L antibonding orbitals in $Cr(CO)_3$ but only one in $\{Rh(PR_3)_2\}^+$: as emphasized in Scheme 2 and Scheme 3, slippage of the former off centre of the ring is prevented by loss of overlap of between the π system and one of the two M–L σ* orbitals.

The NMR spectra of **8** shows no evidence for haptotropic shifts occurring at room temperature, but once again the equivalence of the Me groups in the *i*Bu substituents indicates a rotation of the RhP_2 fragment about the pseudo-C_6 axis of the coordinated ring. We have located a low-lying transition state for the simple rotation (not shown in Figure 5) only 8 kcal/mol above the ground state. Turning to the haptotropic shift, the potential energy landscape is now somewhat different to that described for naphthalene and pyrene because coordination to the mid-point of the central ring is energetically unfavourable. We have located a pathway where the metal migrates from one outer ring to another via intermediate **Trip3** which lies 12.3 kcal/mol above the equilibrium structure. **Trip 3** is structurally very similar to **Trip2**, the only difference being that the metal coordinates to a butadiene fragment on an external edge rather than on the interior. All Rh–C bond lengths are rather long in **Trip2**, but their asymmetry is typical of an

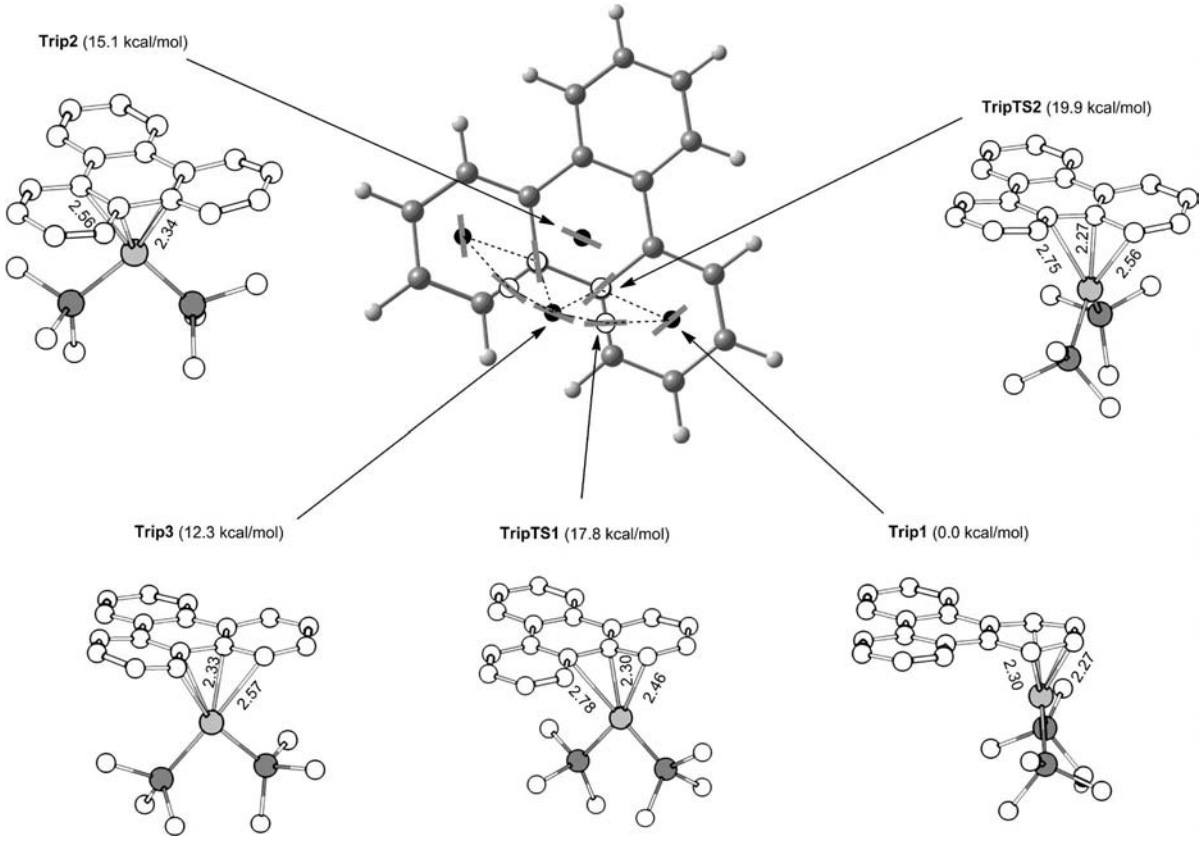

Figure 5. Schematic potential energy surface and structures of stationary points for the triphenylene complex.

η^4-coordination mode. Once again we have located two distinct pathways linking the equilibrium structure to the intermediate, the higher energy one involving a glide of the RhP_2 fragment (**TripTS2**), while the more more accessible corresponds to a glide with concomitant rotation (**TripTS1**). **TripTS1** is structurally rather similar to the η^3-**NapTS2** and **PyrTS1**, with a short central Rh–C bond (2.30 Å) and two rather longer terminal Rh–C distances (2.46 and 2.78 Å). The computed barriers for naphthalene (16.3 kcal/mol), pyrene (11.7 kcal/mol) and triphenylene (17.8 kcal/mol) are fully consistent with the observation that only the pyrene complex is fluxional at room temperature.

Coronene: $[Rh(PMe_3)_2(C_{24}H_{12})]^+$

The global minimum for the coronene structure, **Cor1**, reproduces the experimentally observed η^2-geometry with encouraging accuracy (Figure 6). The T-shaped Rh centre, inequivalent Rh–P bonds and coordinated C=C bond perpendicular to the P–Rh–P plane are also strikingly similar to those in the archetype complex of ethene, **Eth1**. The stability of the 14-electron configuration at the metal, whilst initially surprising, can be rationalised by the dominant Clar structure for free coronene with its three resonant sextets and three isolated C=C double bonds. Coordination to an isolated C=C double bond therefore results in minimal disruption to the π system, an observation that is confirmed by the computed NICS values. The adoption of alternative η^3 or η^4 coordination modes, while increasing the electron count at the metal, would necessarily entail a much more substantial disruption of the aromatic π system.

The lowest energy pathway connecting any two of the six equivalent η^2 minima is typical of the migration/rotation pathways described above for naphthalene and pyrene, with an η^3-coordinated intermediate, **Cor3**, lying only 8.8 kcal/mol above the global minimum, **Cor1**. The transition state connecting **Cor1** and **Cor3**, **CorTS1**, is very similar to the intermediate, both structurally and energetically (ΔE = 8.9 kcal/mol). We have also located a direct "glide" transition state, **CorTS2**, where the $\{Rh(PMe_3)_2\}^+$ fragment translates without concomitant rotation, but this again lies somewhat higher in energy (ΔE = 13.2 kcal/mol). Transit via the central ring appears to be disfavoured as the η^6 intermediate, **Cor2**, lies +13.0 kcal/mol above **Cor1**, with an intervening transition state at 17.0 kcal/mol. The computed barrier of only 8.9 kcal/mol is the lowest of the four systems discussed here, suggesting that migration should be rapid at room temperature. We have, however, been unable to verify this experimentally as decoordination of the PAH occurs above 200 K.

Transition State Stabilization vs. Ground-State Destabilization

Our survey of the potential energy surfaces for haptotropic shifts shows that the rate-limiting barriers for the

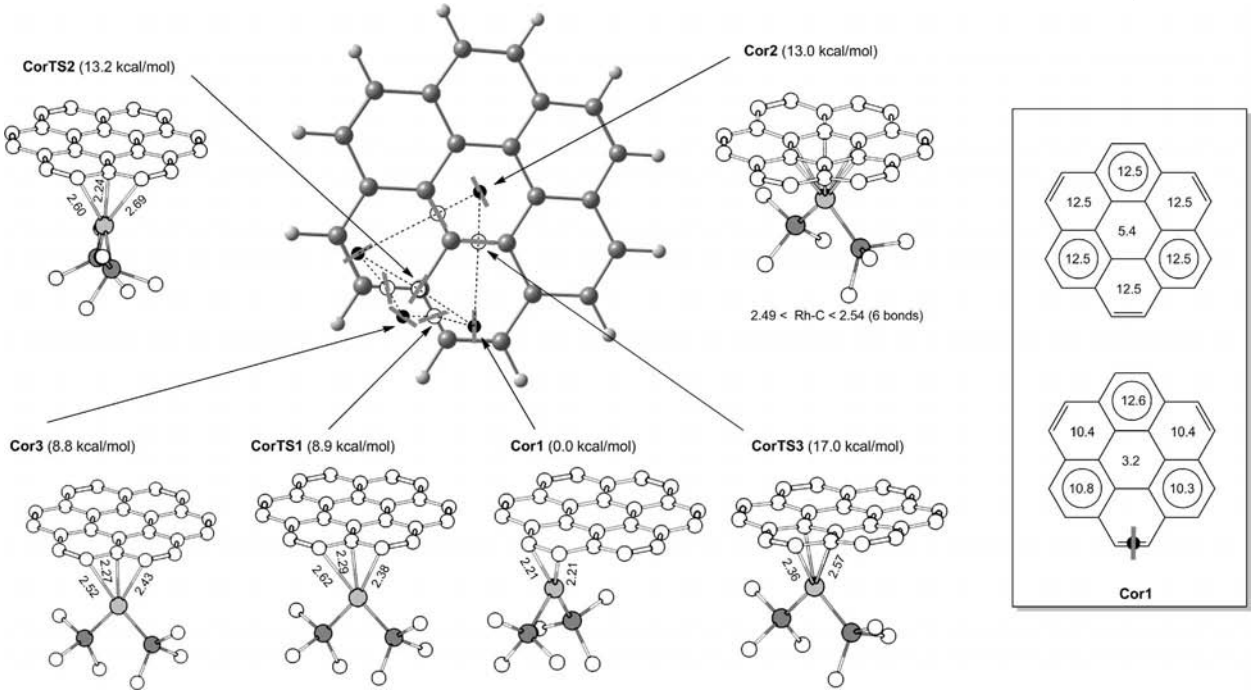

Figure 6. Schematic potential energy surface and structures of stationary points for the coronene complex. NICS(1) values for the uncoordinated rings in key minima are shown in the inset.

pyrene and coronene systems (11.7 and 8.9 kcal/mol, respectively) are ca. 5 kcal/mol lower than those for naphthalene and triphenylene (16.3 and 17.8 kcal/mol, respectively), data that correlate well with the fact that only pyrene has been shown to be fluxional at 210 K (note that decomposition of the coronene complex occurs above this temperature in solution, so its fluxionality has not been established). The height of a barrier is, of course, defined by the relative energies of equilibrium and transition states, and it is important to establish whether variations across the series are primarily a result of changes in the former or the latter – i.e., is the low barrier in pyrene a result of transition state stabilization or ground-state destabilization? Trends in the computed dissociation energies [–42.7 kcal/mol (naphthalene), –39.7 kcal/mol (pyrene), –43.3 kcal/mol (triphenylene) and –39.0 kcal/mol (coronene)] correlate directly with the barrier heights, suggesting that differences in the ground state are key. In support of this suggestion, we note that the transition states are structurally rather similar (all are weakly bound allyl-like structures) while variations in equilibrium structures are more pronounced. Thus in cases such as naphthalene and triphenylene where a 16-electron configuration can be attained without major disruption to the aromatic π system, large dissociation energies and high barriers ensue. In the pyrene and coronene complexes, in contrast, a compromise is unavoidable in the equilibrium structure, leading to low dissociation energies and low barriers. It is important to emphasise that this trend maps directly onto the laboratory observation that complexes of pyrene (**7**) and coronene (**9**) can only be formed in the presence of excess ligand, and start to decompose in solution at temperatures much above 200 K.

Conclusions

This paper has set out a detailed computational analysis of haptotropic shifts using a $\{Rh(P\textit{i}Bu_3)_2\}^+$ fragment bound to progressively larger PAH ligands. Whilst studies of isolated compunds have been reported previously, this represents the first attempt to approach the graphene limit in a systematic way. The convergence of experiment (structure and VT NMR) and theory is impressive, and leads to a deep understanding of the processes involved. The very different behaviour of the naphthalene, pyrene, triphenylene and coronene systems is determined by the electronic demands of the metal (favouring a 16-electron configuration) and ligand (favouring retention of maximal aromatic conjugation). In cases where these two demands can be met simultaneously (naphthalene, triphenylene), the result is an energetically isolated equilibrium structure and large barriers to migration. In the pyrene and coronene systems, in contrast, a compromise is inevitable with either the metal centre or the aromatic unit in a less than optimal configuration. This instability is manifested in the presence of more than one structure in solution, low barriers to haptotropic shifts and facile dissociation of the ligand.

Computational Methodology

All calculations were performed using the BP86 functional[20] with the Gaussian03 series of programs.[21] Rhodium and phosphorus were described with SDD basis set,[22] while main group atoms were described using the SVP basis.[23] An extra set of *f*-polarisation functions was added to the Rh (αf = 1.350) along with a set of d-polarization function (αd = 0.387) for phosphorus.[24] Unrestricted

geometry optimizations were carried out in each case, and stationary points were confirmed to be genuine minima or transition states by analytical calculation of their harmonic vibrational frequencies. The Nucleus-Independent Chemical Shifts (NICS) values were calculated at the BP86, SDD on Rh and P and cc-pVTZ on C and H[25] level using the GIAO (Gauge-Independent Atomic Orbital) method as recommended by Schleyer et al.[12] The NICS probes were placed 1 Å above the centres of the rings (defined as the average of the Cartesian coordinates of the rings atoms) [NICS(1)]. The NICS(1) values largely reflect the influence of π-electrons, and are therefore a better indicator of the ring current (aromaticity) than the values at the centre, where σ-bonding contributions are also important.

Supporting Information (see footnote on the first page of this article): Complete set of Cartesian coordinates for all computed structures.

Acknowledgments

We thank the Oxford Supercomputing Centre (OSC) for provision of computational facilities and the Iraqi Ministry of Higher Education and Scientific Research (MoHESR) for a scholarship (to M. A. M. A.).

[1] A. Woolf, A. B. Chaplin, J. E. McGrady, M. A. M. Alibadi, N. Rees, S. Draper, F. Murphy, A. S. Weller, *Eur. J. Inorg. Chem.* **2011**, 1614–1625 (preceding paper).
[2] T. A. Albright, P. Hofmann, R. Hoffmann, C. P. Lillya, P. A. Dobosh, *J. Am. Chem. Soc.* **1983**, *105*, 3396–3411.
[3] C. C. Romao, L. F. Veiros, *Organometallics* **2007**, *26*, 1777–1781; J. O. C. Jimenez-Halla, J. Robles, M. Sola, *Organometallics* **2008**, *27*, 5230–5240.
[4] J. O. C. Jimenez-Halla, J. Robles, M. Sola, *J. Phys. Chem. A* **2008**, *112*, 1202–1213.
[5] K. H. Dötz, J. Stendel, S. Muller, M. Nieger, S. Ketrat, M. Dolg, *Organometallics* **2005**, *24*, 3219–3228; S. Ketrat, S. Muller, M. Dolg, *J. Phys. Chem. A* **2007**, *111*, 6094–6102; A. Pfletschinger, M. Dolg, *J. Organomet. Chem.* **2009**, *694*, 3338–3342.
[6] Y. F. Oprunenko, N. G. Akhmedov, D. N. Laikov, S. G. Malyugina, V. I. Mstislavsky, V. A. Roznyatovsky, Y. A. Ustynyuk, N. A. Ustynyuk, *J. Organomet. Chem.* **1999**, *583*, 136–145; Y. Oprunenko, I. Gloriozov, K. Lyssenko, S. Malyugina, D. Mityuk, V. Mstislavsky, H. Gunther, G. von Firks, M. Ebener, *J. Organomet. Chem.* **2002**, *656*, 27–42; J. Pan, J. W. Kampf, A. J. Ashe, *Organometallics* **2006**, *25*, 197–202; L. Turker, S. Gumus, *Acta Chim. Slov.* **2009**, *56*, 246–253.
[7] F. Nunzi, F. Mercuri, A. Sgamellotti, N. Re, *J. Phys. Chem. B* **2002**, *106*, 10622–10633; F. Nunzi, F. Mercuri, F. De Angelis, A. Sgamellotti, N. Re, P. Giannozzi, *J. Phys. Chem. B* **2004**, *108*, 5243–5249.
[8] G. Zhu, K. E. Janak, J. S. Figueroa, G. Parkin, *J. Am. Chem. Soc.* **2006**, *128*, 5452–5461.
[9] E. Kirillov, S. Kahlal, T. Roisnel, T. Georgelin, J. Y. Saillard, J. F. Carpentier, *Organometallics* **2008**, *27*, 387–393.
[10] J. Silvestre, T. A. Albright, *J. Am. Chem. Soc.* **1985**, *107*, 6829–6841.
[11] E. Clar, *Polycyclic Hydrocarbons*, Academic Press, London, **1964**; E. Clar, *The Aromatic Sextet*, Wiley, New York, **1972**.
[12] P. V. Schleyer, C. Maerker, A. Dransfeld, H. J. Jiao, N. Hommes, *J. Am. Chem. Soc.* **1996**, *118*, 6317–6318.
[13] H. J. Jiao, P. V. Schleyer, *J. Phys. Org. Chem.* **1998**, *11*, 655–662.
[14] M. Guell, J. Poater, J. M. Luis, O. Mo, M. Yanez, M. Sola, *ChemPhysChem* **2005**, *6*, 2552–2561.
[15] J. Muller, P. E. Gaede, C. Hirsch, K. Qiao, *J. Organomet. Chem.* **1994**, *472*, 329–335.
[16] M. A. Bennett, Z. B. Lu, X. Q. Wang, M. Bown, D. C. R. Hockless, *J. Am. Chem. Soc.* **1998**, *120*, 10409–10415.
[17] R. Boese, A. Stanger, P. Stellberg, A. Shazar, *Angew. Chem. Int. Ed. Engl.* **1993**, *32*, 1475–1477.
[18] R. H. Mitchell, Y. S. Chen, N. Khalifa, P. Z. Zhou, *J. Am. Chem. Soc.* **1998**, *120*, 1785–1794; R. H. Mitchell, *Chem. Rev.* **2001**, *101*, 1301–1315; D. V. Simion, T. S. Sorensen, *J. Am. Chem. Soc.* **1996**, *118*, 7345–7352; F. Feixas, J. O. C. Jimenez-Halla, E. Matito, J. Poater, M. Sola, *Pol. J. Chem.* **2007**, *81*, 783–797.
[19] M. A. Bennett, M. Bown, D. C. R. Hockless, *Aust. J. Chem.* **2000**, *53*, 507–515.
[20] A. D. Becke, *Phys. Rev. A* **1988**, *38*, 3098–3100; J. P. Perdew, *Phys. Rev. B* **1986**, *33*, 8822–8824.
[21] M. J. Frisch, G. W. Trucks, H. B. Schlegel, G. E. Scuseria, M. A. Robb, J. R. Cheeseman, J. A. Montgomery, T. Vreven, K. N. Kudin, J. C. Burant, J. M. Millam, S. S. Iyengar, J. Tomasi, V. Barone, B. Mennucci, M. Cossi, G. Scalmani, N. Rega, G. A. Petersson, H. Nakatsuji, M. Hada, M. Ehara, K. Toyota, R. Fukuda, J. Hasegawa, M. Ishida, T. Nakajima, Y. Honda, O. Kitao, H. Nakai, M. Klene, X. Li, J. E. Knox, H. P. Hratchian, J. B. Cross, V. Bakken, C. Adamo, J. Jaramillo, R. Gomperts, R. E. Stratmann, O. Yazyev, A. J. Austin, R. Cammi, C. Pomelli, J. Ochterski, P. Y. Ayala, K. Morokuma, G. A. Voth, P. Salvador, J. J. Dannenberg, V. G. Zakrzewski, S. Dapprich, A. D. Daniels, M. C. Strain, O. Farkas, D. K. Malick, A. D. Rabuck, K. Raghavachari, J. B. Foresman, J. V. Ortiz, Q. Cui, A. G. Baboul, S. Clifford, J. Cioslowski, B. B. Stefanov, G. Liu, A. Liashenko, P. Piskorz, I. Komaromi, R. L. Martin, D. J. Fox, T. Keith, M. A. Al-Laham, C. Y. Peng, A. Nanayakkara, M. Challacombe, P. M. W. Gill, B. G. Johnson, W. Chen, M. W. Wong, C. Gonzalez, J. A. Pople, *GAUSSIAN 03*, revision D.02, Gaussian, Inc., Wallingford, CT, **2004**.
[22] D. Andrae, U. Haussermann, M. Dolg, H. Stoll, H. Preuss, *Theor. Chim. Acta* **1990**, *77*, 123–141; A. Bergner, M. Dolg, W. Kuchle, H. Stoll, H. Preuss, *Mol. Phys.* **1993**, *80*, 1431–1441.
[23] A. Schafer, H. Horn, R. Ahlrichs, *J. Chem. Phys.* **1992**, *97*, 2571–2577.
[24] A. Hollwarth, M. Bohme, S. Dapprich, A. W. Ehlers, A. Gobbi, V. Jonas, K. F. Kohler, R. Stegmann, A. Veldkamp, G. Frenking, *Chem. Phys. Lett.* **1993**, *208*, 237–240; A. W. Ehlers, M. Bohme, S. Dapprich, A. Gobbi, A. Hollwarth, V. Jonas, K. F. Kohler, R. Stegmann, A. Veldkamp, G. Frenking, *Chem. Phys. Lett.* **1993**, *208*, 111–114.
[25] T. H. Dunning, *J. Chem. Phys.* **1989**, *90*, 1007–1023; R. A. Kendall, T. H. Dunning, R. J. Harrison, *J. Chem. Phys.* **1992**, *96*, 6796–6806; D. E. Woon, T. H. Dunning, *J. Chem. Phys.* **1993**, *98*, 1358–1371.

Received: December 2, 2010
Published Online: February 21, 2011

